Copyright Warning & Restrictions

The copyright law of the United States (Title 17, United States Code) governs the making of photocopies or other reproductions of copyrighted material.

Under certain conditions specified in the law, libraries and archives are authorized to furnish a photocopy or other reproduction. One of these specified conditions is that the photocopy or reproduction is not to be "used for any purpose other than private study, scholarship, or research." If a, user makes a request for, or later uses, a photocopy or reproduction for purposes in excess of "fair use" that user may be liable for copyright infringement,

This institution reserves the right to refuse to accept a copying order if, in its judgment, fulfillment of the order would involve violation of copyright law.

Please Note: The author retains the copyright while the New Jersey Institute of Technology reserves the right to distribute this thesis or dissertation

Printing note: If you do not wish to print this page, then select "Pages from: first page # to: last page #" on the print dialog screen

ABSTRACT

PRODUCTION OF SUBMICRON AEROSOL BY POWDER DEPRESSURIZATION

by
Amit Haryani

Disaggregation of dry powders in shear flow has limitations in producing submicron particles. This study explores a new method for the production of submicron particles by the depressurization of powder aerosols. The depressurization mechanism is based on the rapid depressurization of the aggregated powder through a specially designed nozzle. As the pressure suddenly decreases from very high values inside the aggregates (800 psi) to ambient at the surface of such aggregates, disaggregation takes place due to the force exerted by the gas escaping through their pore structure.

The effect of various process parameters, namely: nozzle diameter, pressure and pretreatment with surfactants were investigated. Comparison of the particle size distribution produced indicated that better disaggregation is achieved with the smaller nozzle diameter. The results showed that a pressure of 100 psi was sufficient to effect disaggregation on powder by overcoming the secondary forces within the aggregates. The product particle size distribution showed a weak dependence on pressure upto 800 psi. The enhancement of disaggregation by surfactants pretreatment was not very significant. This novel method is expected to be significant in the production and processing of submicron and nanoparticles.

PRODUCTION OF SUBMICRON AEROSOLS BY POWDER DEPRESSURIZATION

by
Amit Haryani

A Thesis
Submitted to the Faculty of
New Jersey Institute of Technology
In Partial Fulfillment of the Requirements for the Degree of
Master of Science in Environmental Engineering

Department of Civil and Environmental Engineering

May 1999

APPROVAL PAGE

PRODUCTION OF SUBMICRON AEROSOLS BY POWDER DEPRESSURIZATION

Amit Haryani

Dr. Mohamed E. Labib, Thesis Advisor — Date
Research Professor of Civil and Environmental Engineering,
New Jersey Institute of Technology, Newark, NJ

Dr. Taha Marhaba, Committee Member — Date
Associate Professor of Civil and Environmental Engineering,
New Jersey Institute of Technology, Newark, NJ

Dr. Robert Pfeffer, Committee Member — Date
Professor of Chemical Engineering,
New Jersey Institute of Technology, Newark, NJ

BIOGRAPHICAL SKETCH

Author: Amit Haryani

Degree: Master of Science in Environmental Engineering

Date: May 1999

Undergraduate and Graduate Education:

- Master of Science in Environmental Engineering
  New Jersey Institute of Technology, Newark, NJ, 1999

- Bachelors of Technology (Chemical),
  Indian Institute of Technology, Bombay, India. 1996

Major: Environmental Engineering

This thesis is dedicated to my loving parents
and my beloved guru Sri Sri Ravishankar.

ACKNOWLEDGMENT

The author would like to express his deepest appreciation to Drs. Mohammed E. Labib and S. Dukhin, who not only served as research supervisors, providing valuable insights and intuitive suggestions, but also provided constant encouragement and reassurance. The author offers his special thanks to Dr. Taha Marhaba and Dr. Pfeffer for serving as members of the committee.

The author would also like to express his thankfulness to Dr. E. Baygi, Dr. Y. Ding, Mr. Chandrakant Patel, and Dr. S. Mukherjee for their assistance over the duration of the research. Lastly the author would like to thank all his colleagues and friends for their moral support.

TABLE OF CONTENTS

TABLE OF CONTENTS
(Continued)

Chapter **Page**

TABLE OF CONTENTS
(Continued)

Chapter **Page**

LIST OF TABLES

Table **Page**

LIST OF FIGURES

Figure **Page**

CHAPTER 1

INTRODUCTION AND THEORY

During the past decade, submicron and nanoparticles and their properties have attracted attention of researchers from many disciplines. The term *submicron* is generally used to indicate particles with diameter between 100 nm to 1μm; and, the term *nanoparticles* is generally used to indicate particles with diameters less than 100 nm. Submicron and nanoparticles are suitable for many functional applications, including: advanced ceramics, advanced composites, superconductors and catalysts. An important example of functional nanostructure relates to chemical reactions between nanoparticles for fast energy release such as in case of solid fuels. This thesis focuses on the disaggregation of powders to produce submicron particles using a novel method based on the depressurization of the aerosols.

1.1 Submicron Particle Synthesis Methods

The methods used to produce submicron particles can be broadly classified into four types: a.) dispersion (breakup) of solid bodies, b.) gas phase synthesis methods, c.) solution phase synthesis methods and d.) combined dispersion and solution phase methods.

The various synthesis methods involved in the disaggregation of powders include *high energy mechanical milling and mechanical attrition*. The most commonly used mechanical mills are: fine impact and vibration mills (1). For fine impact mills, grinding

takes place through impact and collision between the aggregates and impact element. In this process, the aggregates are normally accelerated in a fast gas stream. During the collision with the impact element the kinetic energy of aggregates breaks them into smaller aggregates. The type of mechanical action preferred in vibrational mills is a combination of beating, impact and friction. To achieve high fineness of the product, vibration mills are generally operated wet, since the dry process promotes aggregation and agglomeration of the powder which impede the grinding process with increasing particle fineness. Rawers et al. (2) reported that some nanoparticles are produced during mechanical milling and that such nanoparticles are usually attached to the submicron particles. Endo et al. (3) have investigated the disaggregation of several kinds of fine powder aggregates consisting of polydispersed aggregates by application of *shear flow*. They used nitrogen gas at high pressures (0.3 – 10 MPa) to accelerate the aggregates to a critical velocity of about 280 m/s. The accelerated particles were then passed through a specially designed convergent-divergent nozzle. The disaggregated powder was then collected by sedimentation in a collection chamber. The above authors were able to break the large aggregates into smaller aggregates with average aggregate diameter of 1 μm. They observed that only a part of the kinetic energy was used for disaggregation of powder using shear flow. Higashitani et al. (4) have reported that the average size of these broken aggregates and the maximum number of constituent particles in a broken aggregate can be successfully expressed as a function of the energy dissipation in the nozzle.

1.2 Surface Forces and Adhesion in Aggregates

A *primary aggregate* is composed of primary particles rigidly held together by solid bridges, whereas agglomerate usually consists of primary particles and/or aggregate held together by relatively weak forces (7). The Cohesive strength of agglomerate depends on the packing of its constituents and also on the strength of the interparticle interaction within the agglomerate. It is now well established that electromagnetic and gravitational interactions are the primary forces that act between atoms and molecules. With the development of quantum theory it was possible to understand the origin of intermolecular forces and also the phenomenon of interparticle attraction. It is now well established that all intermolecular forces are electrostatic in origin. This is encapsulated in the Hellman-Feynman theorem. Unfortunately, difficulty to obtain the exact solution of the Schrodinger equation for complex cases leads to classification of interparticle and intermolecular forces as ionic forces, van der Waals forces, hydrophobic interactions, hydrogen bonding and solvation forces. These interparticle forces lead to aggregate formation.

Particles are usually characterized by the single particle dimensions. This characterization is not sufficient because powders are almost always aggregated, except for the cases when they are stabilized with a surfactant layer during synthesis (5). If the particles are not protected by surfactant adsorption, any collision is accompanied with aggregation. The latter results in *primary aggregates* consisting of 10 to 100 particles, depending on the nature of attractive forces. Inert gas phase condensation is a commonly used method for particle production. Its mechanism includes evaporation of a metal followed by cooling that causes high supersaturation and homogeneous nucleation. The

primary aggregates arise in parallel with singlet's growth during nucleation, suggesting that the condensation process may comprise the contacts between singlets as well. As a result of condensation contacts, the dispersability of primary aggregates is low and they are difficult to break.

This collision of primary aggregate leads to aggregation of primary aggregates, resulting in the formation of *secondary aggregates*. The contacts between primary aggregates within secondary aggregates are caused by colloidal forces responsible for coagulation. These forces are weaker and hence secondary aggregates are easier to break.

The notion of primary and secondary aggregates is an over simplification. The real and more exact structure of aggregates is modeled by the fractal theory of aggregates. Fractal geometry is a tool by which simple rules can be used to construct realistically complex objects like the structure of a powder aggregate. Structural characterization in terms of fractal geometry is playing an increasingly large role in studies of porous materials. Crawford et al. (6) have studies the relation between the number-size distribution and the dimension of fractal aggregates. Meakin (7) has proposed a model that relates the surface geometry and fractal dimensions to parameters of history, properties and behavior. These parameters play an important role in disaggregation, since the structure of aggregates is expected to determine their response to mechanical and other external forces. Knowledge of surface structure of a pore helps predict phenomena of capillary condensation and water-bridge formation that play a crucial role at high pressures and close to saturation. Hence, the need arises to define the fractal geometry of powders with respect to their disaggregation behavior under external mechanical forces.

1.3 Influence of Structural Heterogeneity on Breakup of Agglomerate

As discussed in the previous section, the transmission of stress within an aggregate and hence its tendency to break under hydrodynamic shear, strongly depends on the arrangement of the primary particles within aggregate. Most existing models of disaggregation of aggregates, usually treat the structure of an aggregate as a uniformly porous sphere or as a uniform assembly of spheres. The fracture of such aggregates is usually envisioned to occur along planar surfaces. Horwatt et al. (8) have reported that the experimental observations of the breakup of aggregates demonstrate that a variety of fragment sizes were produced from the rupture of a parent aggregate. They also reported a large difference between the disjoining forces observed experimentally and those predicted on the basis of measurements of the cohesive strength of the solids. The authors investigated the disaggregation of aggregates using five types of computer-generated aggregate structures and found that heterogeneity of structures accounts for such large discrepancy

Intuitively, fragments will form according to the location of internal packing heterogeneity's present within the parent agglomerate. These correspond to both the weak portion of the agglomerate (where the agglomerate might first fail), as well as to strong portions (which resist disaggregation). Bang et al. (9) have studied the heterogeneity of the particle size distribution (PSD) of powders and emphasized the importance of multimodal particle size distribution in theses cases. For a multimodal distribution, the authors found that the particles of each size range have different agglomerate strengths. Also, they found that a multimodal PSD can be approximated with two or three distinct log-normal distributions, each corresponding to a different agglomerate strength. In our

case, this phenomenon of intragglomerate heterogeneity could manifest itself in the form of multimodal distributions.

1.4 Disaggregation in Shear Flow

For a long time, there was a notion that the disaggregation of powders in a fast gas stream cannot be efficient with respect to submicron particles. It was recently confirmed that this method was efficient only with particles with dimension, micron or larger (3). The authors have reported the limitations of the shear flow mechanism with respect to the production of submicron particles. With the use of a specially designed convergent-divergent nozzle, the author succeeded to disaggregate powders consisting of 1 micron particles.

The necessary condition for disaggregation via shear flow mechanism is the presence of a velocity gradient. This is represented in figure 1.1

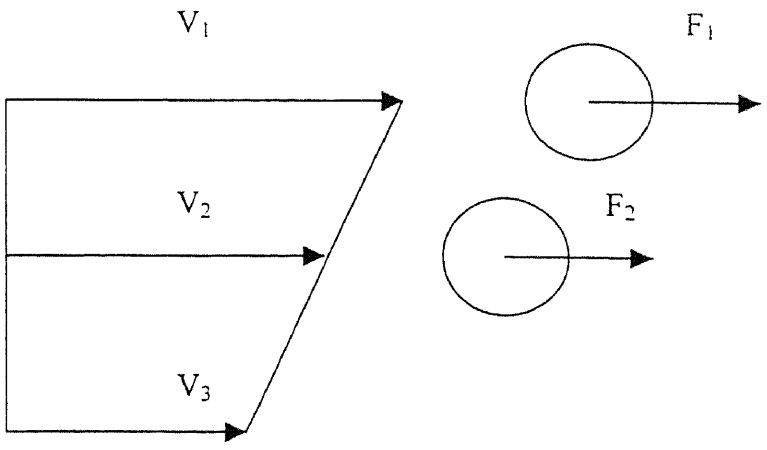

Figure 1.1 Shear force on a particle due to velocity gradient.

It is known that the shear force, F, is proportional to the velocity V.

Hence,

$$\text{Disaggregation Force} = F_1 - F_2 \propto V_1 - V_2$$

In the fast gas stream method (3) this velocity gradient is provided by a special long nozzle that is designed to provide maximum shear forces. It can be demonstrated that the velocity gradient is absent in short-narrow nozzle, as in our case. In a long nozzle the gradient arises near surface due to the flow retardation by wall surface, i.e., the velocity near the surface of nozzle is zero and gradually increases to a maximum at the center. However, in the nozzle entrance the velocity distribution is uniform over the entire crossection. This uniform distribution preserves along a part of initial section of the nozzle. The length of this section can be evaluated by the application of the theory of aerodynamic boundary layer. This boundary layer arises due to velocity retardation along the wall of nozzle. The thickness of the boundary layer is zero at the entrance and gradually increases along the length of the nozzle. Velocity gradient manifests itself in this boundary layer. However, the increase in thickness of the boundary layer is very slow and as result a long nozzle length is required to achieve the required velocity gradient for the shear force to be effective.

The length of the nozzle needed to provide the required velocity gradient is calculated as follows:

$$L = 0.1 \times \mathrm{Re} \times d \tag{1.1}$$

where Re is the Reynolds Number and d is the diameter of the nozzle. If the nozzle length, l, is smaller than this length, L, shear flow mechanism does not manifest itself.

These considerations were taken into account during our nozzle design to study the depressurization methods-i.e., we use a short-length nozzle where shear forces are not significant compared to forces generated due to depressurization.

1.5 Inefficiency of the Fast Gas Stream Method (Shear Flow) in Disaggregating Submicron and Nanoparticles

The yield strength of an aggregate can be estimated as $F_b/(\Pi r^2)$, where the bonding force of coagulated particles within the aggregate, F_b, is proportional to the particle radius (r) (3,11). As a result, the yield strength for submicron aggregates is expected to be 10 to 100 times larger than for aggregates consisting of micron-size particles. For aggregates moving under a velocity gradient, the velocity difference for 2 points with 2r distance between them equals 2rV, where V is the stream velocity gradient (10). The force required to disintegrate these aggregated particles is then proportional to the distance squared.

$$F_{12} = 12\pi\eta r^2 V \tag{1.2}$$

To separate particles from an aggregate, the disjoining forces, F_{12}, applied to adjacent particles (within such aggregate) must exceed the bonding forces, F_b, between these particles. F_b decreases linearly with the particle radius r, while a stronger than proportional dependence holds for F_{12}, i.e., it decreases even faster, as shown by the above equation. Hence disaggregation becomes increasingly difficult for smaller particles. Figure 1.2 shows forces acting on a particle as a function of interparticle distance.

The above force decreases more rapidly, than the adhesion force, with decreasing particle dimension. Hence for submicron particles, the velocity gradient of upto 100 to 1000 times larger is needed to provide disaggregation, compared to that needed for the micron-size particles. This is difficult to achieve by conventional techniques. Hence, we propose a new depressurization mechanism to provide efficient disaggregation of powders in the submicron and nanometer range.

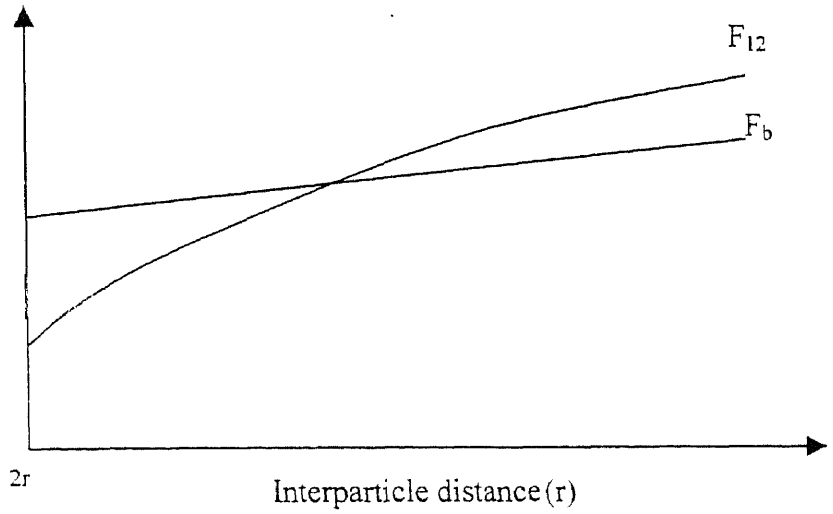

Figure 1.2 Forces acting on a particle as a function of interparticle distance

1.6 Principle of Depressurization Mechanism

This phenomenon is based on a straightforward experimental arrangement where the aggregates are filled with a gas inside a pressure vessel, followed by the rapid depressurization of the gas through a special discharge nozzle. At any moment, the pressure inside the aggregate exceeds the pressure near its surface, which is equal to the pressure inside the discharge nozzle. The latter decreases along the length of the discharge nozzle. As a result, the pressure difference between the aggregate center and

its surface increases along the discharge stream, i.e., along the length of the discharge nozzle. Under certain conditions, the aggregates will be subjected to sufficient forces to break them up into smaller agglomerate and singlets. In our case a short-length nozzle is used to maximize this pressure drop.

When the internal pressure decreases very slowly in comparison to the external pressure, the situation can be considered as an invariant pressure inside aggregate, with the rapid decrease of pressure only across the last two external layers. As a result the pressure gradient can be evaluated as the pressure drop divided by the particle dimension. For a pressure of 100 atm and particle dimension 100 nm, the pressure gradient of 10^7 atm/cm arises. This extremely high pressure gradient provides the separation of the external layer from the aggregate. Hence, layer by layer an aggregate can be disintegrated almost completely. This scenario, of course, depends on the nature of the microstructure of the aggregate under construction.

1.7 Break-Up Modes of the Aggregates

Depending on the magnitude of the adhesion forces between the particles, the aggregates are expected to breakup in different modes. In case of weak adhesion forces, the disaggregation proceeds in layers, starting with external layer and moving towards the center of the aggregate, as shown in Figure 1.3. The pressure gradient inside an aggregate is maximum at the outer surface. The removal of the external layer reveals the underlying layer, for which again the pressure gradient is maximal. Hence, the process is repeated and layered disaggregation continues.

On the other hand, when large adhesion forces bind the particle, the entire aggregate will break in two or more parts under influence of the total pressure drop ΔP. Under influence of this gradient, the first – or couple – of layers separate from the aggregate and split into singlets, doublets or smaller agglomerates, as shown in Figure 1.4.

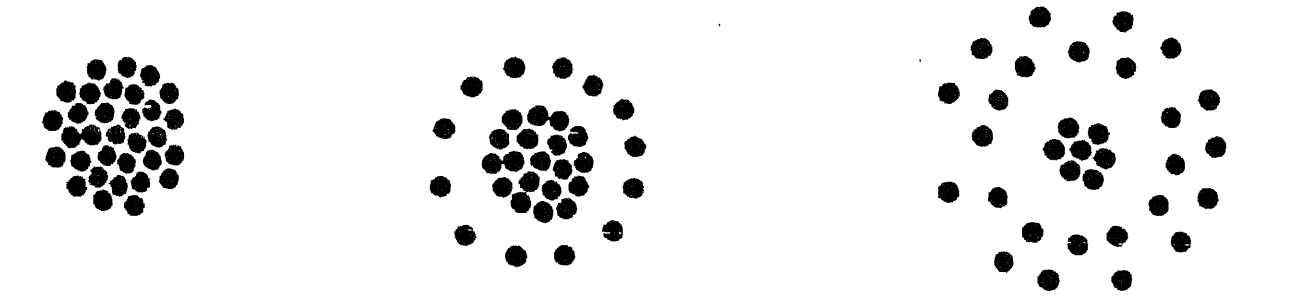

Figure 1.3 Layered disaggregation

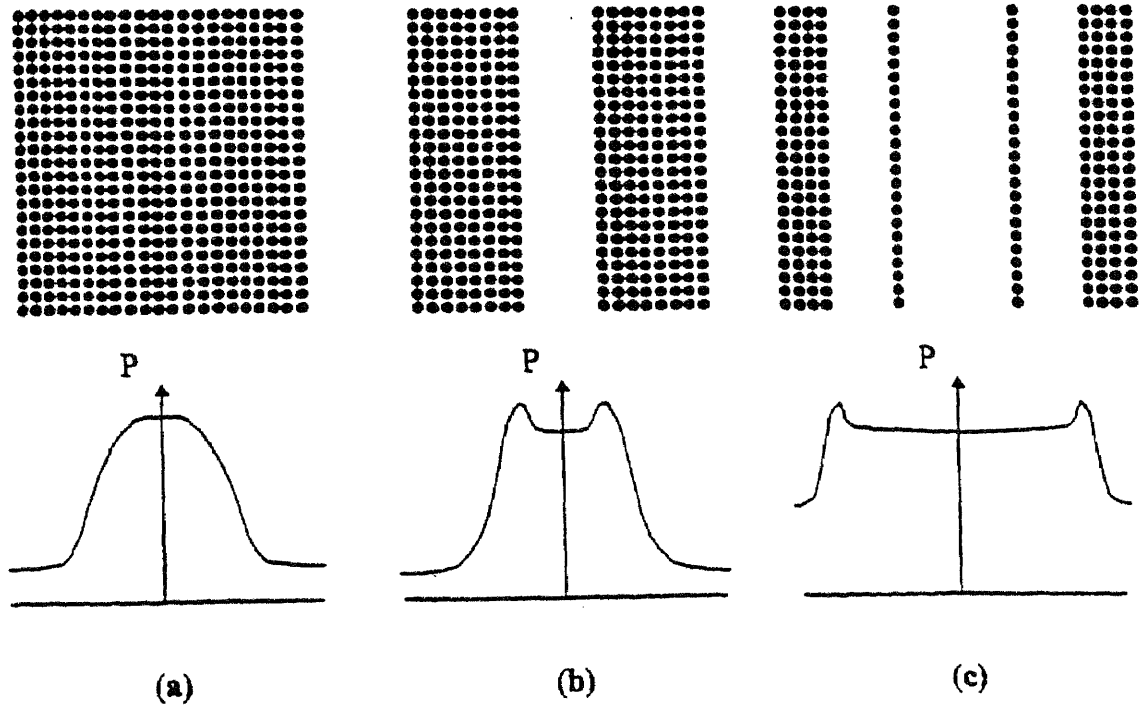

Figure 1.4 Stages and pressure distribution in the disaggregation process

1.8 A Mathematical Model for Compressed Gas Release from Aggregates

During depressurization of aggregates at least two stages may be discriminated. The initial stage leads to the destruction of the contacts between particles in the aggregate. During this stage the pressure gradient inside the aggregate and the disjoining force F_{12} increases. As F_{12} exceeds F_b, the particles start to separate from each other in the aggregate. Thus during the first stage, the aggregate can be considered as a rigid body with gas flowing through it under a pressure gradient. During the second stage, the contacts between particles have been broken, and both gas and particles move at different rates, i.e. a multicomponent flow manifests itself.

Using the theory of unsteady compressible fluid flow through a porous medium, the necessary condition for disaggregation during the first stage is found to be:

$$F_{12}(r,t) = F_b \tag{1.2}$$

The equation for the characteristic time of compressed gas release from an aggregate was derived as:

$$\tau_{ag} = \frac{\eta}{Pf(\gamma)}\left(\frac{l}{r}\right)^2 \tag{1.3}$$

where η, P, l and r are: viscosity, pressure in the vessel, aggregate radius and particle radius respectively. $\gamma = \Phi^{1/3}$ where Φ is the particle volume part in the aggregate and $f(\gamma)$ is the coefficient characterizing the aggregate hydrodynamic resistance dependence on its porosity.

The fast compressed gas release from aggregates leads to a fast pressure decrease inside them. To define the conditions needed for aggregate breakup in the discharge nozzle during gas release, two characteristic times must be introduced:

1. time of aggregate gas release τ_{ag}

2. time of depressurization in the discharge nozzle

The optimal condition for disaggregation is satisfied when the aggregate release time exceeds the depressurization time in the discharge nozzle. In this case, the initial high pressure in the aggregate is preserved during the depressurization through the discharge nozzle. In many cases, this optimal condition is difficult to realize even during the most rapid depressurization along the discharge nozzle --- about 1 microsecond. The latter is realized at high velocity (almost sound velocity), and with the use of narrow discharge nozzle, 100 micron in diameter.

Examination of several scenarios indicated that the conditions depend on particle dimensions. The larger the particles in the aggregate and correspondingly, the wider the pores, the smaller is the hydrodynamic resistance and the more rapid the depressurization takes place, i.e. smaller aggregate depressurization characteristic time. For submicron and nanoparticles, the aggregate depressurization time increases 100 times or more according to equation (1.3) and exceeds the nozzle discharge depressurization characteristic time of 1 microsecond. Hence, the large difference between the pressure inside an aggregate and its surface can be realized in this process, and therefore disaggregation can be achieved.

1.8.1 Micro-Rheological Model of Aggregates

This model relates the internal rheological behavior of the aggregates to the parameters characterizing their inner structure. The aggregate is assumed to be spherical and consist of spherical nanoparticles. The local velocity of gas filtration in the aggregate, under the influence of the local pressure gradient, was expressed by means of hydrodynamics at low Reynolds number (4):

$$u = \frac{f(\gamma, r)}{\eta} \cdot \frac{dP}{dR} \tag{1.5}$$

where R represents the radial coordinate assigned to the aggregate.

1.8.2 Gas Release from an Aggregate During Depressurization

Due to extremely narrow pores, viscous forces are dominant. Inertial forces can be neglected because the characteristic time

$$\tau_k = \frac{d^2}{32\mu} \tag{1.6}$$

is shorter than the gas release time τ_{ag}, μ and d are the kinematic viscosity and the diameter of the pores respectively. The time τ_k represents a lower limit, above which a quasi-steady approximation of the gas flow is valid. In this case, taking the spherical symmetry of the system into account, the continuity equation for compressible flow is:

$$\frac{\partial \rho(R,t)}{\partial t} = \frac{1}{R^2} \frac{\partial}{\partial R} \left[R^2 \rho(R,t) u(R,t) \right] \tag{1.7}$$

The density distribution is represented by $\rho(R,t)$ and the velocity u(R,t) is given by (1.5). Equation (1.7) can be linearized due to the fact that the disaggregation occurs in the entrance section of the discharge nozzle, where the pressure drop is considerably smaller than the initial pressure in the aggregates. The latter is equal to the pressure in the vessel P_v. After Linearization and assuming an isothermal process, (1.7) becomes:

$$\frac{\partial P}{\partial t} = \frac{N}{R^2}\frac{\partial}{\partial R}\left[R^2\frac{\partial P}{\partial R}\right] \tag{1.8}$$

with

$$N = \frac{r^2 f(\gamma) P_v}{\eta} \tag{1.9}$$

where P_v is the pressure in the vessel, η is the kinematic viscosity of gas.

Knudsen and Katz (12) have reported that the pressure in the entrance section of the discharge nozzle decreases linearly over a length Δz, i.e. during the time $t=\Delta z/v$, where v is the flow velocity in the discharge nozzle. Since the gas release is assumed to take place during this time, the boundary condition for (1.8) can be written as

$$P(l,t) = P_v - \Delta P\frac{t}{\tau} \tag{1.10}$$

where τ is gas release time

The solution of the parabolic expression (1.8) for a non-steady boundary condition is achieved by means of Duhamel integral (8). The general solution for a spherical system was obtained by Knudsen and Katz (12).

By specifying this solution for the condition (1.10), the pressure distribution in the aggregates as a function of time was obtained. The pressure drop between the aggregate center and its periphery can be expressed as

$$\frac{P(0,t)-P(l,t)}{\Delta P}=\frac{2l^2}{\pi N}\sum_{n=1}^{\infty}(-1)^{n-1}\frac{1-\exp(-n^2\pi^2 Nt/l^2)}{n^2\pi^2} \qquad (1.11)$$

By comparing (1.11) and (1.4), the sufficient condition for the realization of the pressure drop ΔP can be derived as $\tau_{ag} > 10\tau$.

1.9 Objectives of Work

The main objective of this research was to define the critical parameters for studying depressurization as a new method for disaggregating submicron and nanoparticles. Hence, the study was carried out to achieve the following objectives:

1. To find an optimum powder loading condition.
2. To study the effect of pressure on the degree of disaggregation
3. To study the effect of nozzle diameter on the degree of disaggregation.
4. To study the effect of using of surfactant-coated powder on disaggregation.
5. To compare the results to a shear flow mechanism, as per literature coverage (8).
6. To investigate different types of powders to demonstrate the generality of powder disaggregation by the depressurization method.

1.10 Organization of the Thesis

In Chapter 2, we discuss aspects of aerosol mechanics and design parameters needed to configure our experimental apparatus. In Chapter 3, we discuss the powders, methods and experimental set-up used to acquire data presented in this thesis. In Chapter 4, we present and discuss the results of the experiments carried out in our laboratory and provide a general understanding of the processes involved in disaggregation by the depressurization mechanism. In Chapter 5, we provide conclusions of our study; and in Chapter 6 we suggest the scope for improvement in future research.

CHAPTER 2

DESIGN OF EXPERIMENTAL APPRATUS

2.1 Design of a Experimental Set-Up (Figure 2.1)

Compressed air obtained from the S.O.S. gas company (industrial grade) was used as the depressurization fluid. The depressurization experiments were performed in a 115ml stainless steel pressure vessel rated to withstand 10.000 psi. To prepare for an experiment, the vessel was opened from both ends and washed with methanol to remove any powder left from the previous experiment. The vessel was then dried in a jet of air. Typically, 23 mg of powder was introduced into the vessel with a spatula. The vessel was then connected to the air cylinder at one end and to the nozzle, through a valve, at the other end. The inlet valve was opened to fill the pressure vessel with air to a particular pressure. The outlet valve, as shown in *Figure 2.1*, was opened and the gas was allowed to pass through the nozzle. The online particle size analysis of the disaggregated aerosol particles stream was made by the (API Aerosizer).

2 Experimental Set-Up Design and Mechanics of Aerosol

2.2.1 Selection and Design of the Nozzle

A smaller nozzle diameter has the advantage that it maximizes both velocity gradient and the depressurization time. As discussed in section 1.4, shear mechanism can be realized in a long nozzle only. Depressurization mechanism, on the other hand, can be realized in a short-length nozzle. The aerodynamic resistance of a long nozzle is very large, leading

to decrease in velocity. However, for a large gas velocity to be manifested, the aerodynamic resistance has to be small, i.e., the length of the nozzle has to be small. Hence, to avoid high resistance and loss of velocity, the use of short nozzle is necessary. Hence, experiments were conducted with 100, 300, 600 and 1000 micron diameter nozzles, respectively. The l/d ratio of the nozzles was 5, 1.6, 0.8 and 0.5 respectively. Where l is the length of the nozzle and d is the diameter of the nozzle.

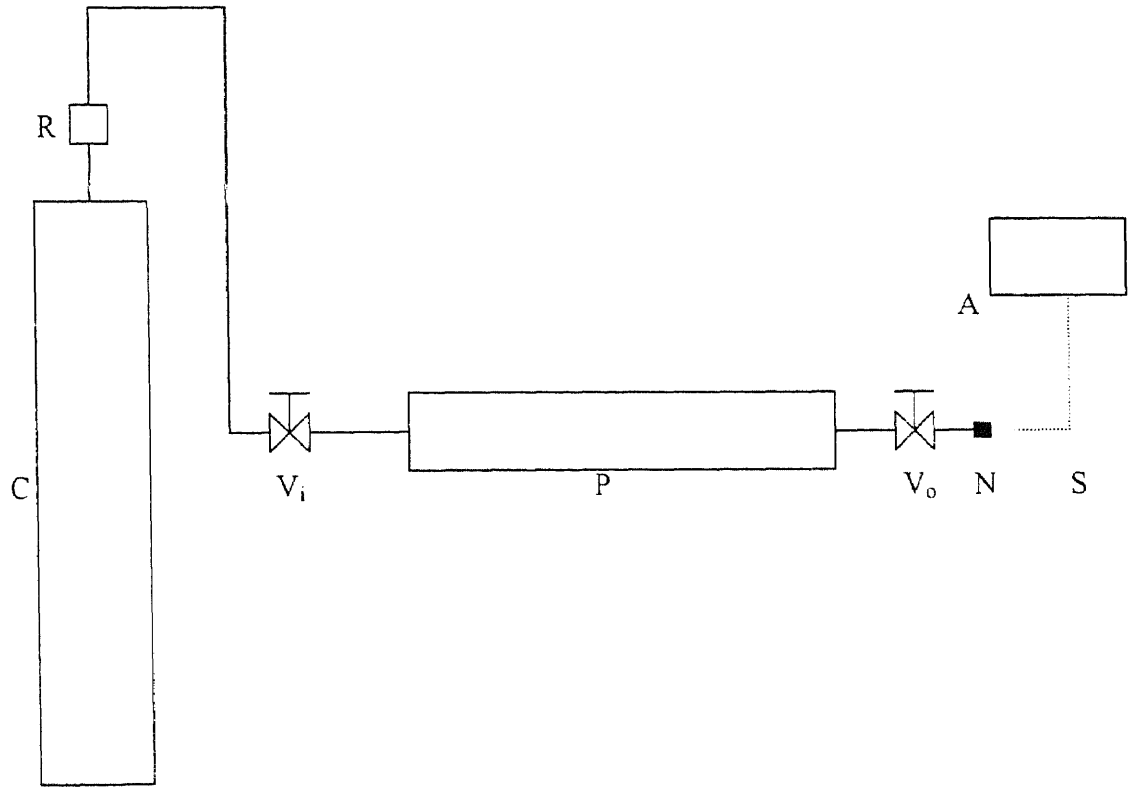

C - Compressed Gas Cylinder, R - Pressure Regulator, V_i - Inlet Valve, P - Pressure Vessel, V_o - Oulet Valve, N - Orifice, S - Sampling Tube, A - Online API Aerosizer

Figure 2.1 Schematic Diagram of the Experimental Apparatus

2.2.2 Sampling of the Aerosol Stream

The particle size analysis of the generated aerosol stream exiting the nozzle was done using the API Aerosizer. A sampling tube connected to the Aerosizer was used for online measurements of the aerosol stream. If the sampling tube is placed at an angle to the direction of flow, then some deposition takes place on the wall of the tube due to inertia. So the concentration of the sample measured may represent less than the true concentration of the aerosol entering such tube. The suction generated by the Aerosizer introduces another complication in sampling the correct aerosol concentration: this additional pressure drop would produce larger concentration at the sampling point of the Aerosizer. This has the disadvantage that the increased concentration leads to coagulation of the particles in the sampling tube and consequently a shift in the particle size distribution to the right – i.e., larger particle size is observed. As the aerosol moves in the sampling tube, precipitation of the particle takes place along the walls of the tube. Fuchs (11) has found that the length of the tube, L_{cr}, required for complete precipitation is given as:

$$L_{cr} = \frac{2h\bar{U}}{V_s} \tag{2.1}$$

where, h is half the height of the tube, $\bar{U}$ is the mean velocity and V_s is the sedimentation velocity of the particle. For the aerosol stream generated by depressurization experiments, the length of tube needed for complete precipitation is 300-m. The actual length of the sampling tube used in the experiments is 0.5 m. Hence, losses due to sedimentation can be neglected.

2.2.3 Sedimentation in the Vessel

When the gas from the cylinder is introduced into the pressure vessel, the particles become aerosolized but if this aerosol is left undisturbed, some of the particles settle to the bottom. Fuchs (11) reported that, for an infinitely long cylindrical vessel of radius R, the average concentration of the particles, $\bar{n}$, at time t is given by:

$$\bar{n} = 4n_0 \sum_{\nu=1}^{\infty} \frac{1}{\beta_\nu} e^{-D\beta_\nu^2 t / 2R} \qquad (2.2)$$

where β_1, β_2 ..... are the zeros of the zero-order Bessel functions of the first kind $I_0(x)$, which have the following values: $\beta_1^2 = 5.784$; $\beta_2^2 = 30.47$; $\beta_3^2 = 74.89$; $\beta_4^2 = 132.8$; $\beta_5^2 = 222.9$. n_0 is the initial concentration of particles in the vessel. If the residence time of the gas in the vessel is long then some of the suspended particles are lost due to sedimentation. For this reason, optimization effort was made to reduce the time between vessel pressurization and gas release. This was achieved by reducing the time between pressurization of vessel and aerosol release through the nozzle.

2.2.4 Deposition of the Aerosol in Turbulent Flow

Experimental studies of the distribution of mean velocities for turbulent flow in pipes and open channels have shown the existence of a logarithmic velocity profile $U = a \ln z + b$ where U is the mean velocity at a distance z from the wall. Deposition in a turbulent stream can be either diffusive or inertial in nature. Fuchs (11) proposed for diffusive deposition from turbulent flow, that the number of particles, I, passing in 1 second through 1 cm^2 of surface parallel to the wall:

$$I = \frac{\beta D^{3/4} n_0 \mathrm{Re}_f^{7/8} \nu^{1/4}}{57R} \tag{2.3}$$

Where D is eddy diffusion coefficient

ν is the Kinematic eddy Viscosity

β is a numerical coefficient (~1).

R is the Radius of the tube.

n_0 is the initial concentration of the aerosol.

Also, a flow round an obstacle (such as parts of the nozzle and other parts of the sampling hardware) gives rise to vortices, as shown in figure 2.2.

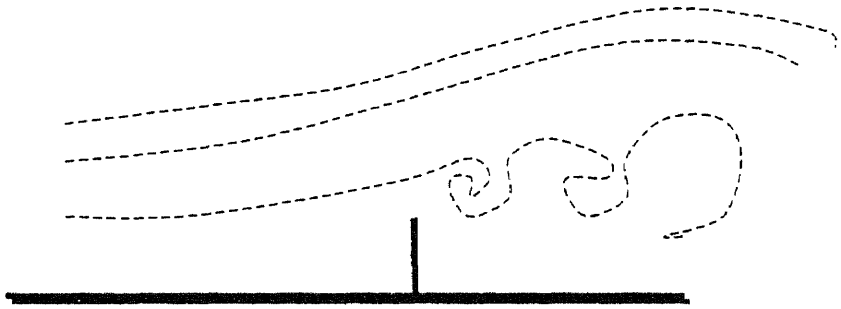

Figure 2.2 Flow of gas close to an obstacle (11).

This causes inertial deposition of aerosols from the turbulent stream to take place. The deposition rate of particles per 1 cm^2 of the wall surface is given as:

$$I = \frac{n_0 U^{*2}}{\bar{U}[1 + U^*(14.5^3 / 2l^{*3} - 50.6]} \tag{2.4}$$

where $l^* = l_i U^* / \nu$, U^* is the friction velocity and $\bar{U}$ is the r.m.s. velocity in the direction normal to the wall at the distance l_i .Hence, the loss of suspended particles is expected at the nozzle in our experiments which would affect powder concentration in the aerosol stream involved in our measurements.

2.3 Use of Surfactants

Notably, adsorption of surface-active species in the contact zone within an agglomerate can lead to an increase of the distance at the contact points, and therefore can make disaggregation easier during gas depressurization. Considering that van der Waals attraction forces are inversely proportional to the square of the shortest interparticle distance, a decrease in the bonding energy between particles, by factor of 10 or more may be realized by adsorption of surfactant species.

Husemann et al. (1) have used surfactants for experiments on disaggregation of aggregates by ultrafine grinding. They reported that the use of surfactants had positive effect and resulted in lower energy consumption during the grinding process. The effect of surfactant addition was studied on a very cohesive material such as limestone and resulted in a marked reduction of internal friction and thus improved the flowability of the limestone powder. Hence, an improvement in disaggregation in our case may be anticipated if the aggregated powder is pretreated with a surfactant prior to the disaggregation experiments.

For this purpose, two anionic, surfactants were employed, namely: Sodium bi(2-ethyl hexyl) Sulfosucconiate (AOT) and Sodium Dodecyl Sulfate.

CHAPTER 3

MATERIALS AND METHODS

3.1 Materials

The powders used in this study were experimental grades of titanium dioxide, fumed silica (L-10) powders supplied by the Sutimoto Corporation. Some important properties of the powder are summarized in *table 3.1* below.

Table 3.1 Properties of powders used for depressurization experiments.

Powder	Primary Particle Size* (nm)	Absolute Density (g/cm^3)
Titanium dioxide	25	4.5
Fumed silica	16	2.2

* This is the size of individual particle in a fused aggregate, *See* section 3.4.2

The surfactants employed were sodium di(2-methyl hexyl) sulfosuccionate (AOT) and sodium dodecyl sulfate (SDS) from Aldrich Company. Some surfactant properties are summarized in *Table 3.2.*

Table 3.2 Properties of surfactants used for powder treatment prior to depressurization.

Surfactants	Chemical Formula	Solubility Parameter(δ) $(cal/cm^3)^{1/2}$	M Wt. (g/mol)
AOT	$CH_3(CH2)_3CH(C_2H_5)CH_2OOCCH(SO_3Na)$ $COOCH_2CH(C_2H_5)(CH_2)_3CH_3$	8.2	444.0
SDS	$C_{12}H_{25}SO_4Na$	8.1	288.4

3.2 Powder Treatment with Surfactants

Toluene was used to adsorb AOT onto the powder. SDS was adsorbed by dissolving in methanol. The choice of solvent was made in order to prevent any water-bridge formation that would negatively affect the disaggregation of the powder. 1 mg of the surfactant was dissolved in the 10 cc of solvent. 2.5 gm of TiO_2 was suspended in the 10 cc of solvent and mixed with the surfactant solution to make the total volume to 20 cc. The solution was sonicated for 5 minutes and then dried in an oven for 24 hour. The sedimented cake was broken up manually and preserved in a dessicator before use in the disaggregation experiments.

3.3 Particle Size Distribution Analysis

3.3.1 API Aerosizer®

We used the Amherst Process Instruments (API) Aerosizer® for particle size distribution analysis of the aerosol stream generated from the nozzle. The instrument is based on the time of flight aerosol beam spectrometry (TOFABS). The TOFABS method consists of (a) dispersing sample particles in a gas such as air to form an aerosol sample, (b) accelerating the aerosol as part of an expanding gas jet, such as in air expanding through a nozzle into an evacuated chamber wherein the air jet accelerated, (c) detecting at discrete locations the passage of individual particles in a narrow, high-speed beam of particles i.e. in an aerosol beam formed in the expanding transonic jet and (d) counting the time-of-flight of each particle between detection locations. The particle size range of this instrument can be as low as 100 nm.

3.3.2 Light Scattering Particle Size Analyzer of Liquid Dispersion of Powders

We used the 90Plus particle size analyzer made by the Brookhaven Instruments Corporation for characterizing powders for the purpose of comparing with the results of the depressurization method. The particle size analyzer is based on light scattering technique using a Helium-Neon laser as the light source. The scattered light is collected at a 90-degree angle to the incident light source. The photon correlation spectroscopy of quasi-elastically scattered light technique, based on correlating the fluctuations about the average scattered light intensity, is the basis of this measurement mechanism. The instrument can measure particles as low as 30 nanometers.

3.4 Experimental Scope

3.4.1 Experiments for System Parameters Characterization

The experiments were conducted at pressures of 100, 500, 800 and 1200 psi respectively, to study the dependence of PSD on pressure. The effect of nozzle diameter was studied by using different nozzles of 1mm, 0.6mm, 0.3mm and 0.1 mm diameters, respectively; nozzles were supplied by Precision Orifices Corporation. Experiments were also conducted with different powder loading to study the effect of powder loading on disaggregation, and to obtain an optimized powder to gas ratio for best disaggregation. Also, experiments were conducted with surfactant-coated powders to study the effect of surfactant on this disaggregation method.

3.4.2 Experiments for Particle Characterization

As discussed in Section 3.3.1, the 90Plus Particle size analyzer was used to find the ultimate particle size of disaggregated powders. The experiments performed involved dispersing of the powder in methanol, followed by sonication for 5 minutes. The sample was then analyzed using the 90Plus Particle size Analyzer. The PSD obtained for TiO_2 showed a monodispered distribution with average primary aggregate diameter of 172 nm. The PSD obtained for fumed silica showed a multimodal distribution with average particle size of 525 nm. The mean particle diameter of 172 nm for TiO_2 and 525 nm for fumed silica are much bigger than that reported by the manufacturer. Hence, it is concluded that the particle dimensions provided by the manufacturer represent the diameter of primary particles and that these primary particles exist in the form of fused aggregates.

3.4 Analysis of PSD used in Quantifying Effectiveness of Disaggregation

When a powder is subject to disaggregation, the mean size and mass fraction of the larger constituents gradually diminish, while the mass fraction of smalle-size constituents gradually increase. Assuming that the bulk density of the powder remains unaffected by disaggregation, an attempt was made to normalize the data collected, on volume basis. Thus a unit volume of base powder is expected to transform into a large number of smaller particles as a result of disaggregation. A sample calculation for the normalized data is given in Appendix A

CHAPTER 4

RESULTS AND DISCUSSION

4.1 Effect of Powder Loading on Disaggregation

To study the effect of powder loading, experiments on disaggregation of powders through depressurization were done using fumed silica (L-10) at 1200psi and with orifice of 0.3 mm diameter. The PSD results obtained from the Aerosizer indicated that the particle size range was narrower for 6.5 mg powder loading compared to higher loadings of 23 mg and 51 mg. *Figure 4.1* shows the PSD of disaggregated particles obtained at different powder loadings, after being normalized with respect to volume. No particles were detected by the Aerosizer in the size range 100 to 200 nm, for 6.5 mg powder loading. However for the 23 mg powder loading, high particle number count was found for the size range100 to 200 nm. In general, it was also observed that the higher powder loading leads to a shift of the PSD towards the higher size range. Higher particle loading is expected to lead to the production of larger number of disaggregated particles per unit volume of aerosol stream which results in increased collisions between the particles inside sampling tube; this is turn leads to the coagulation of the disaggregated particles in the aerosol stream. The coagulation of particles in the sampling tube may explain the to increase in size of the aggregates measured by the Aerosizer. Coagulation can also manifest itself inside the pressure vessel, as described in section 2.2.2. Since the powder loading of 6.5 mg was inadequate to perform experiments for longer time, 23 mg of powder was used for all subsequent experiments.

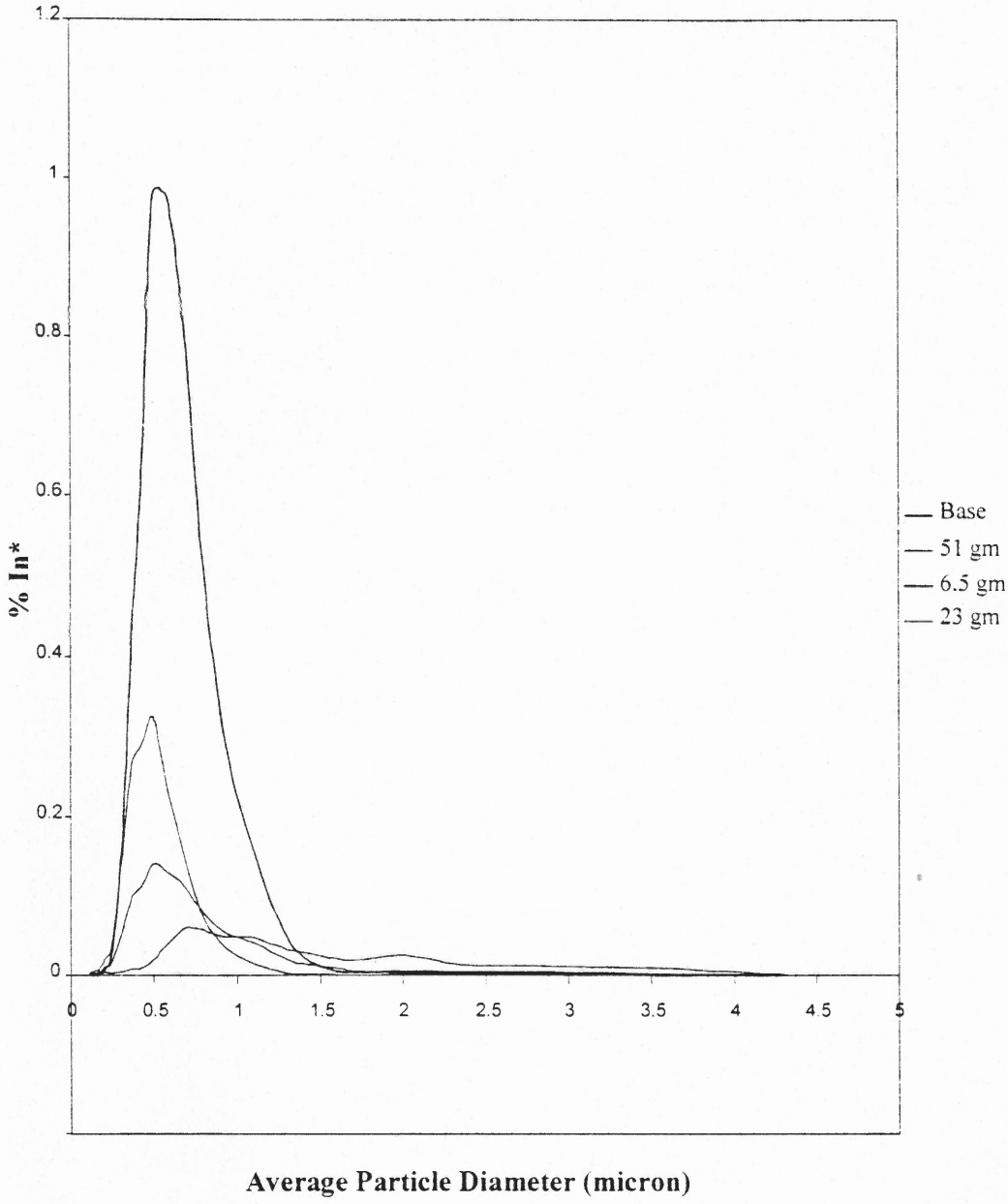

Figure 4.1 Dependence of particle diameter on powder loading for fumed silica powder. (nozzle diameter =0.3 mm; pressure = 1200 psi)

Note: *% In** is % In (% of total number of particles) a size range, normalized for unit volume of sample.

Base represents data for experiments base particle size

6.5 gm represents data for experiments with 6.5 gm powder loading.

23 gm represents data for experiments with 23 gm powder loading.

51 gm represents data for experiments with 51 gm powder loading.

4.2 Effect of Nozzle Diameter on Disaggregation

As discussed in Section 1.3 the length of the capillary needed for the shear flow mechanism to manifest is given by Equation 1.1.

$$L = 0.1 \times \mathrm{Re} \times d \tag{1.1}$$

For our experiments, assuming that the diameter of the orifice is 100 micron, kinematic viscosity of air equals 0.15 cm^2/s, and velocity of the gas stream equals 300 m/s. Then the Reynolds number equals 2000. Hence, according to equation 1, the length of capillary needed to manifest shear flow would be 20 cm. But, our orifice is 0.5 mm in length, suggesting that depressurization is indeed the predominant mechanism.

Figure 4.2 shows the dependence of the PSD on the orifice diameter d, at 100 psi pressure for titanium dioxide powder. It is found that the smaller particles are produced for the smallest nozzle. As discussed in section 1.8 the optimal condition for disaggregation is satisfied when the aggregate release time exceeds the depressurization time in the discharge nozzle. In this case, the initial high pressure in the aggregate is preserved during the depressurization through the discharge nozzle. For a given pressure inside vessel, the velocity of the aerosol stream generated is highest for the smallest nozzle. This results in smallest depressurization time for the smallest nozzle. Hence, the above condition is best realized for the smallest nozzle where we expect to get the smallest particles.

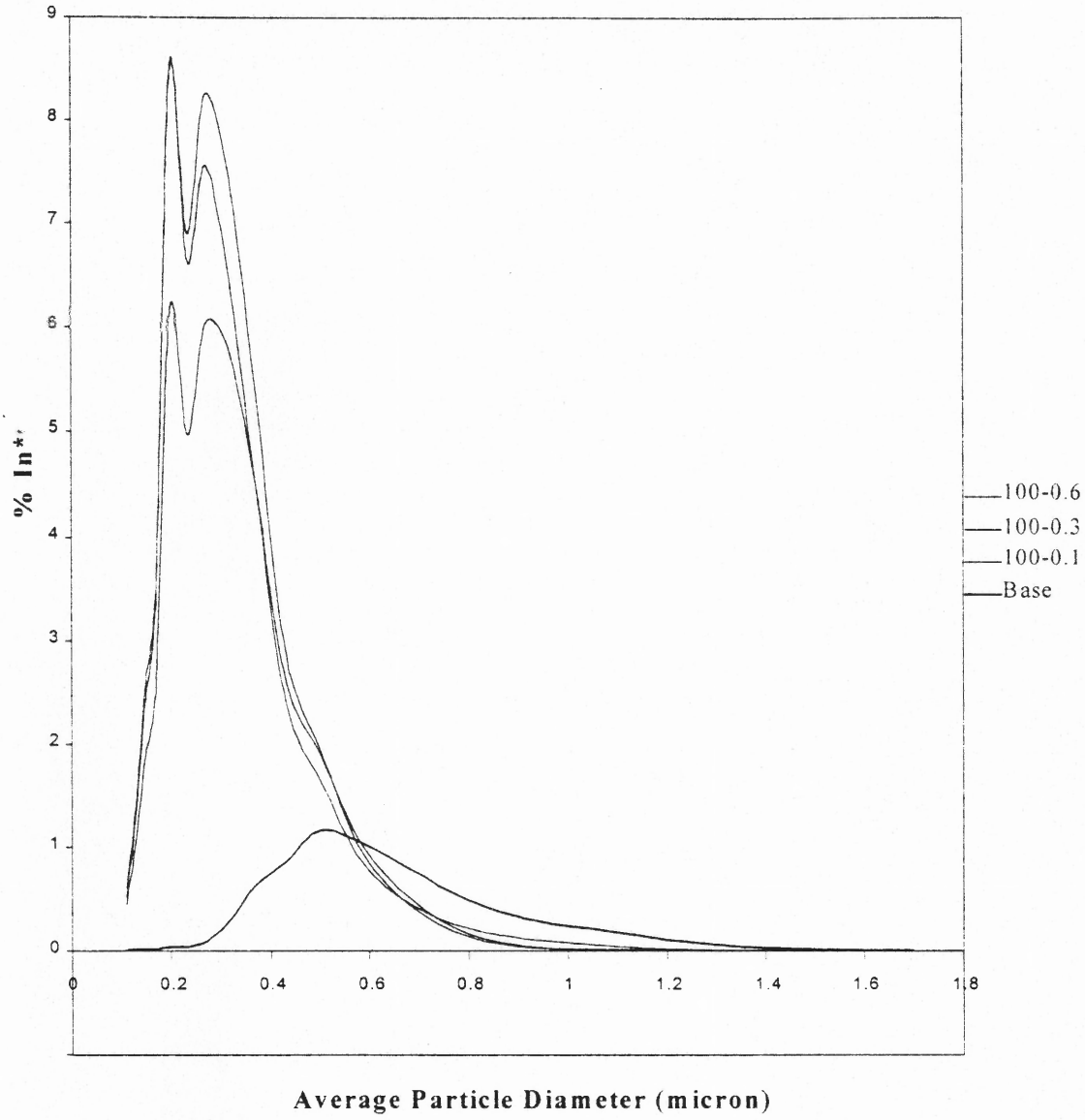

Figure 4.2 Dependence of particle diameter on nozzle diameter for Titanium dioxide powder at 100psi.

Note: *% In** is % In (% of total number of particles) a size range, normalized for unit volume of sample

Base represents data for experiments with base powder.

100-0.1 represents data for experiments at 100psi with 0.1 mm nozzle.

100-0.3 represents data for experiments at 100psi with 0.3 mm nozzle.

100-0.6 represents data for experiments at 100 psi with 0.6 mm nozzle

4.3 Effect of Pressure on Particle Disaggregation

Figure 4.3 shows the dependence of the PSD on the pressure, P, through a 0.3 mm nozzle for fumed silica powder. It is found that the dependence of disaggregation is not very significant, suggesting that even at lower pressures the ultimate disaggregation can be achieved. An increase in pressure by ten folds did not significantly improve the faction of the smaller particles. This suggests that small pressure is sufficient to break the secondary aggregates. Perhaps a rather large pressure drop across the aggregate layers is needed to break the primary aggregates, which could not be realized in the range used in our experiments.

It is interesting to note that the experiments conducted at 800 psi showed better disaggregation compared to those conducted at 1200 psi. This can be explained by the fact that at higher pressure more eddies are generated resulting in higher backmixing and aggregation of the deagglomerated stream. Initially disaggregation improves with increasing the pressure because higher pressure results in larger pressure drop across the aggregates. In our case, this is manifested by the increased numerical concentration for experiment at 800 psi over 100 psi. In addition, as the pressure is increased beyond 800 psi dilution of the aerosol takes place. Hence, at high pressure, decrease in numerical particle concentration due to dilution can be observed as a decrease in total particle numerical concentration, sampled by the Aerosizer, as in the case of 1200 psi. In Conclusion, the clear effect of pressure seems to be complicated by other phenomena occurring during the entire experiment.

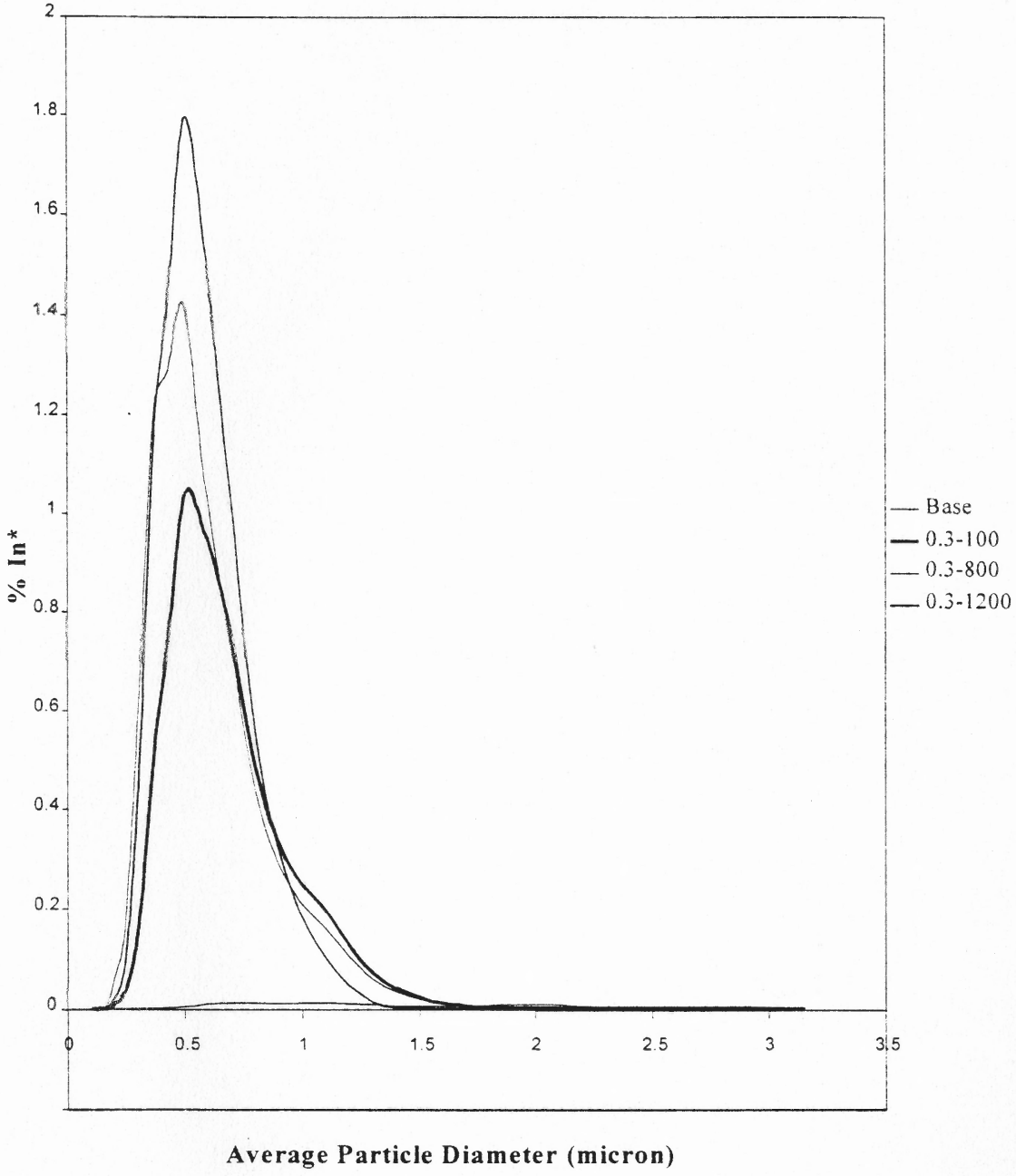

Figure 4.3. Dependence of particle diameter on pressure for fumed silica powder through 0.3 mm nozzle.

Note: *% In** is % In (% of total number of particles) a size range, normalized for unit volume of sample

Base represents data for experiments with base powder.

0.3-100 represents data for experiments at 100psi with 0.3 mm nozzle.

0.3-800 represents data for experiments at 800psi with 0.3 mm nozzle.

0.3-1200 represents data for experiments at 1200 psi with 0.3 mm nozzle

4.4 Effect of Surfactant on Particle Disaggregation

Figure 4.4 shows the effect of surfactant on the PSD for TiO_2 powder at 1200 psi and through 0.3 mm nozzle. As was reported in the section 2.3 surfactants are expected to enhance disaggregation, however, in our study we observed that such enhancement is not appreciable. Both AOT and SDS produced a slight shift in the PSD towards finer particles. This is consistent with the finding of others in the literature.

It is understandable that the nature of surfactant plays an important role in powder disaggregation. Unfortunately, the theory on the influence of surfactants on the interparticle attraction in gas media is absent in the literature. Hence, our choice of surfactant may have not been optimal. The systematic investigation of the influence of different surfactants on disaggregation is beyond the scope of this work, and would itself constitute a topic for an independent work.

The results of this experiment support that disaggregation by depressurization destroys the secondary forces and that surfactant may lie within this type of forces.

4.5 Role of Primary and Secondary Aggregates in Disaggregation Process

Table 4.1 shows average particle diameter of the powder as measured by different instruments. Since ultimate disaggregation can be accomplished in liquid media, the results of Table 4.1 provide the ultimate PSD that can be achieved for these powder. This means that the results produced in methanol dispersion represents the ultimate PSD that can be achieved by breaking up all secondary forces. The latter result was used to judge the effectiveness of the disaggregation by the depressurization method of dry powders used in our experiments.

Table 4.1 Comparison of results obtained for different particle size distribution analyzers.

Powder	Particle diameter (90Plus) (nm)		Particle diameter (Aerosizer) (nm)
	Methanol + Powder	Water + Powder	Dry state
SiO_2	581.9	712.6	620*
TiO_5	173	398.7	240*

Note: * represents diameter of particles with maximum concentration

The experiments for particle characterization using 90Plus particle size analyzer gave mean diameter of 173 nm for sonicated TiO_2 suspended in methanol. This suggests that primary aggregates are present in the powder and that sonication in liquids does not break them.

An average particle diameter of 240 nm and 620 nm were obtained produced by the depressurization method for TiO_2 and fumed silica, respectively. Therefore, it is clear that the primary aggregates cannot be destroyed by depressurization but the secondary forces can be adequately overcome. Therefore, it has been demonstrated through our experimental results that the destruction of the secondary aggregation is efficient. Thus depressurization can be characterized as an efficient disaggregation method, with respect to secondary disaggregation.

With respect to the results of our depressurization experiments, as discussed in section 1.3, a typically multimodal PSD obtained cannot be adequately represented by a

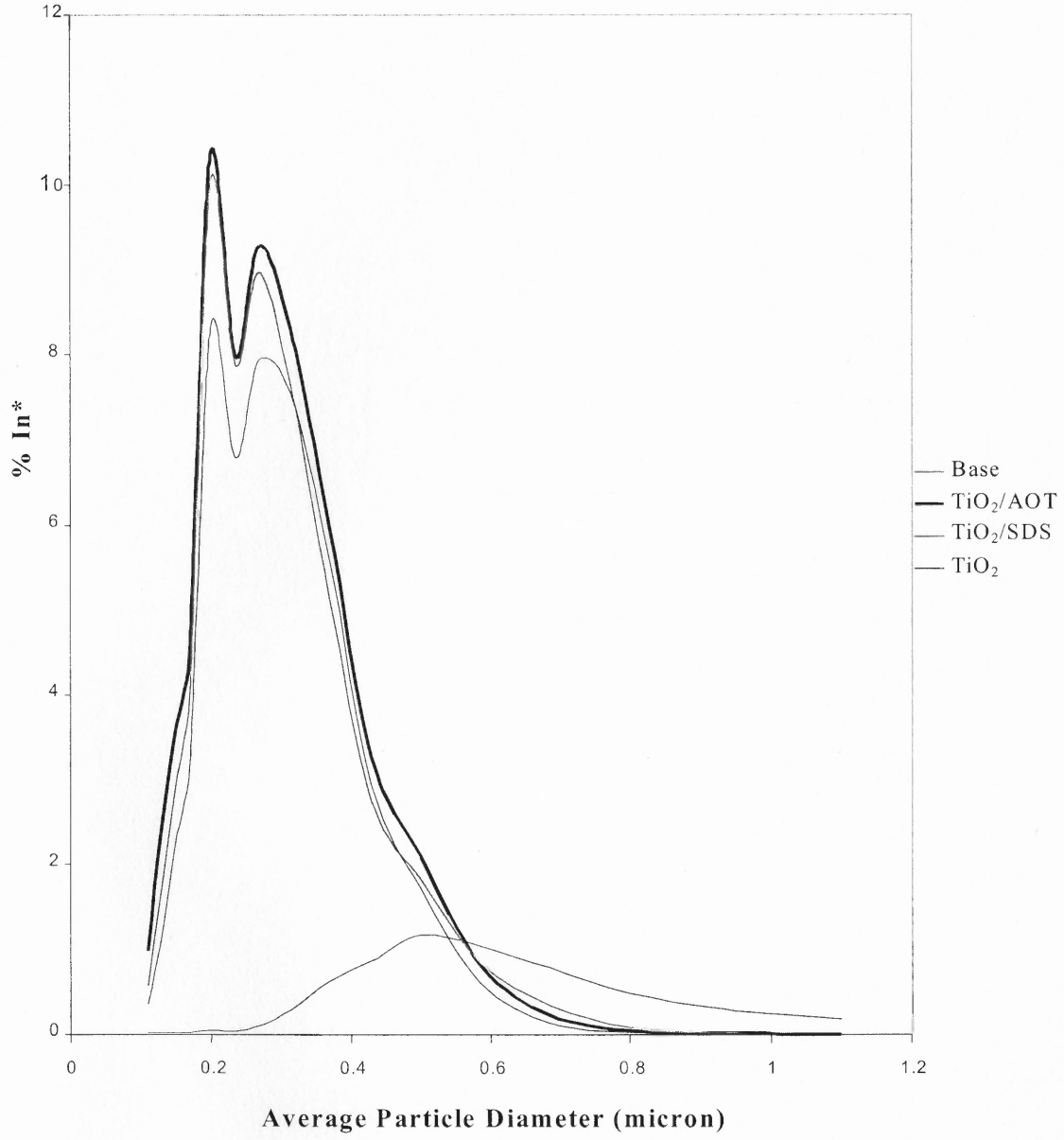

Figure 4.4 Effect of the use of surfactants on particle disaggregation for Titanium dioxide powder. (nozzle diameter = 0.3 mm; pressure = 1200psi)

Note: *% In** is % In (% of total number of particles) a size range, normalized for unit volume of sample

Base represents data for experiments with base powder.

TiO_2 represents data for experiments for Titanium dioxide powder without use of surfactant.

TiO_2/AOT represents data for experiments for Titanium dioxide powder with AOT as surfactant.

TiO_2/SDS represents data for experiments for Titanium dioxide powder with SDS as surfactant

single quantitative value (such as mean diameter). Bang et al. (9) reported that weaker agglomerates break down into smaller particles, while the stronger agglomerates of the same powder remain relatively unchanged giving rise to a multimodal PSD. Horwatt et al (8) have also studied the effect of structural heterogeneity on the breakup of agglomerates in simple shear flow. They have concluded that this structural heterogeneity leads to the formation of variety of fragments depending on the cohesive forces within the agglomerates. The PSD obtained in our study shows a multimodal distribution, which supports the concept of heterogeneity aggregates.

4.6 Depressurization Mechanism *vs* Shear Flow Mechanism

As discussed in section 1.4, a longer nozzle is necessary to provide disaggregation due to shear flow. The velocity gradient needed for shear flow mechanism to be manifested occurs in the boundary layer. The thickness of this boundary layer is very small even for a long nozzle. Hence, only a small part of the aggregates moving in the boundary layer are subjected to disaggregation by shear flow. This limitation due to the boundary layer thickness can be overcome by the use of a long nozzle. But the aerodynamic resistance of the long nozzle is very large leading to low velocity conditions. Thus, it is impossible to satisfy both of the above conditions, i.e., high velocity and non-uniform distribution over the capillary crossection (thick boundary layer). These limitations are inherent in the shear flow mechanism. These limitations however do not exist in the depressurization mechanism, as a small nozzle is sufficient for the realization of the depressurization mechanism. These limitations are reflected in works of other authors. Thus, Endo et al. (3) were able to disaggregate powders upto 1 μm diameter only by the shear flow

method. However, with the use of the depressurization mechanism we were able to produce particles with diameter as small as 200 nm.. We can thus conclude that better disaggregation results are obtained by the depressurization method developed during this study. Indeed perhaps for the first time, particles as small as 200 nm are produced by means of depressurization of dry powders, as in our experiments.

CHAPTER 5

CONCLUSIONS

During this study, a new method for submicron particle generation was developed. In Chapter 1, it was emphasized that nano and submicron particles can only be produced by means of vapor condensation methods or by solution methods involving the adsorption of surfactants during particle formation stages. The production of submicron particles from powders by mechanical and aerodynamic methods is not demonstrated in the literature. This is the first investigation where the possibility of producing submicron particles from aggregated powder by mechanical means is demonstrated. Based on our theoretical evaluation, the shear flow disaggregation mechanism is limited to large-size particles and is not appropriate for the generation of micron or nanoparticles.

The results obtained in this investigation support that the depressurization of powders through an appropriate nozzle, even at 100 psi, was sufficient to breakup secondary aggregates. Comparison of the particle size distribution of disaggregated particles produced at different pressures with that of the parent powder showed a significant enhancement in the number of submicron disaggregated particles with increasing pressure. The highest range of pressure (1200 psi) was insufficient to breakup the primary aggregates. Comparison of the particle size distribution produced by different nozzle diameters indicated that better disaggregation is achieved with smaller diameter nozzle. In conclusion our results demonstrated the destruction of secondary aggregates and the preservation of primary aggregates.

We believe that the analysis of the changes in particle size distribution of a powder after depressurization at pressures above 1200 psi may allow the evaluation of the pressure range sufficient for breaking both secondary and primary aggregates by the depressurization mechanism. Further, the use of a thoroughly dried powder may allow the evaluation of the role of water-bridges on the efficiency of disaggregation process. Finally, the use of a convergent-divergent nozzle would further help to evaluate the effect of nozzle size and shape on the disaggregation process.

The most important factor that may affect the efficiency of this new method relates to the structure of the aggregates; this is expected to determine their response to the mechanical forces generated by the gas escaping through their porous structure. Hence, need arises to define the fractal geometry of powders with respect to their disaggregation behavior by the depressurization method.

CHAPTER 6

SCOPE FOR IMPROVEMENT

6.1 Problems Encountered During Experiments

6.1.1 Powder Loading and Vessel Volume

The powder loading of 23 mg was insufficient to conduct experiments for 90 seconds with 1 mm nozzle. A higher powder loading would be a suitable solution. But as discussed in previous chapter, this generates undesirable results. Hence, we propose to use a vessel with bigger volume and higher powder loading.

6.1.2 Online Measurements

The PSD of the aerosol stream shows a dependence on the distance of the sampling tube of the API Aerosizer from the orifice. Because of the extremely high velocity of the gas stream generated from the orifice, the position of the sampling tube gets disturbed. An improvement to the above situation would be to divide a part of the gas stream and sampling it for PSD.

6.1.3 Higher Pressure

Experiments conducted at 1200 psi with 1 mm orifice require a large volume of gas. The 2200 psi industrial compressed air gas cylinders used were insufficient to carry out multiple experiments. Hence, use of higher pressure compressed gas cylinder is

advisable. This would also give the convenience of performing experiments at much higher pressures and studying the critical pressures needed to break primary aggregates.

6.1.4 Cleaning Procedures

During the experiment, large amounts of fines get deposited on the walls of the sampling tube. This can be translated to a loss of finer particles resulting in poor performance of the system. A cleaning procedure is required to remove these fines before the next set of experiments is performed. With the permanent connection of the sampling tube to the Aerosizer, this seems to be a problem.

6.1.5 Pipe Connections

The vessel, valve and the orifice were opened and cleaned every time, between experiments. Hence, need arises to carefully tighten all the joints, as a leak in the system would necessitate the repetition of the experiment.

6.2 Scope of Improvement

Based on the insight from the experiments conducted and from the work published by others, the following improvements can be made to the existing experimental setup:

6.2.1 Two Vessel System

We propose the use of a two-vessel system. The setup would consist of a primary vessel into which the powder would be fed. The powder would become aerosolized in this first vessel and enters a second vessel, where the sedimentation of large aggregates would take

place. The gas stream from the secondary vessel would be used for depressurization through the nozzle. This arrangement is expected to eliminate many of the problems encountered during this investigation when a one vessel setup was used.

6.2.2 Heating the Depressurization Fluid (Gas)

The effect of water on the PSD was not investigated in the current research. However, many authors have reported that water-bridges are the main cause of agglomerate in dry powders Therefore, it would be advisable to perform the experiments with powders, in the dry condition; experimental setup which would prevent the formation of water bridges that cause aggregation of the produced particles.

6.2.3 Study of Different Powder Systems

The depressurization experiments can be extended to powders. An important system would be the study of depressurization on monodispersed aggregates of different size ranges. This would greatly enhance our understanding of the mechanism especially with respect to this dynamics and transient phenomena involved in the gas flowing through the aggregates and their breakup during depressurization process.

6.2.4 Use of Low Pressure

As has been discussed in the previous chapter, 100 psi is sufficient to break the secondary aggregates. Hence a systematic study of effect of pressures below 100 psi is necessary, to facilitate the understanding of the critical pressure, necessary for secondary aggregate disaggregation.

APPENDIX A

CALCULATIONS FOR NORMALIZATION OF EXPERIMENTAL DATA

Experiment #	100-0.6	100-0.3	100-0.1	Base
# Of Particles	3.07E+07	8.30E+07	3.53E+08	7.85E+06

Lower Size (microns)	Upper Size (microns)	Average Size (microns)	% In a Size Range			
			100-0.6	100-0.3	100-0.1	Base
0.1	0.12	0.11	1.11	1.02	1.26	0.13
0.12	0.14	0.13	2.81	2.77	3.17	0.15
0.14	0.16	0.15	4.79	4.85	5.49	0.17
0.16	0.18	0.17	6.33	6.60	7.32	0.23
0.18	0.22	0.2	15.56	16.73	17.90	0.64
0.22	0.25	0.235	12.49	13.63	13.88	0.61
0.25	0.29	0.27	15.20	16.30	15.84	1.59
0.29	0.34	0.315	14.65	14.88	13.73	4.69
0.34	0.4	0.37	11.35	10.66	9.45	10.52
0.4	0.46	0.43	6.62	5.74	5.07	14.31
0.46	0.54	0.5	4.75	3.82	3.45	19.47
0.54	0.63	0.585	2.55	1.87	1.78	17.21
0.63	0.74	0.685	1.26	0.85	0.93	13.01
0.74	0.86	0.8	0.42	0.26	0.45	8.01
0.86	1	0.93	0.11	0.06	0.24	4.90
1	1.2	1.1	0.02	0.01	0.10	3.00
1.2	1.4	1.3	0.00	0.00	0.02	0.93
1.4	1.6	1.5	0.00	0.00	0.00	0.19
1.6	1.8	1.7	0.00	0.00	0.00	0.05
1.8	2.2	2	0.01	0.00	0.00	0.06
2.2	2.5	2.35	0.01	0.00	0.00	0.05
2.5	2.9	2.7	0.01	0.00	0.00	0.05
2.9	3.4	3.15	0.00	0.00	0.00	0.01

Number in a size range = N

Lower Size (microns)	Upper Size (microns)	Average Size (microns)	Number Of Particles			
			100-0.6	100-0.3	100-0.1	Base
0.1	0.12	0.11	3.4E+07	8.5E+07	4.4E+08	1020500
0.12	0.14	0.13	8.6E+07	2.3E+08	1.1E+09	1193200
0.14	0.16	0.15	1.5E+08	4E+08	1.9E+09	1365900
0.16	0.18	0.17	1.9E+08	5.5E+08	2.6E+09	1805500
0.18	0.22	0.20	4.8E+08	1.4E+09	6.3E+09	5055400
0.22	0.25	0.24	3.8E+08	1.1E+09	4.9E+09	4819900
0.25	0.29	0.27	4.7E+08	1.4E+09	5.6E+09	1.3E+07
0.29	0.34	0.32	4.5E+08	1.2E+09	4.8E+09	3.7E+07
0.34	0.4	0.37	3.5E+08	8.9E+08	3.3E+09	8.3E+07
0.4	0.46	0.43	2E+08	4.8E+08	1.8E+09	1.1E+08
0.46	0.54	0.50	1.5E+08	3.2E+08	1.2E+09	1.5E+08
0.54	0.63	0.59	7.8E+07	1.6E+08	6.3E+08	1.4E+08
0.63	0.74	0.69	3.9E+07	7E+07	3.3E+08	1E+08
0.74	0.86	0.80	1.3E+07	2.2E+07	1.6E+08	6.3E+07
0.86	1	0.93	3254200	4814000	8.3E+07	3.8E+07
1	1.2	1.10	736800	1079000	3.6E+07	2.4E+07
1.2	1.4	1.30	122800	166000	5648000	7316200
1.4	1.6	1.50	30700	0	1059000	1507200
1.6	1.8	1.70	30700	0	0	400350
1.8	2.2	2.00	307000	0	0	471000
2.2	2.5	2.35	276300	0	0	408200
2.5	2.9	2.70	214900	0	0	408200
2.9	3.4	3.15	30700	0	0	54950

Note: Base represents data for experiments with Base particle

100-0.1 represents data for experiments at 100 psi through 0.1 mm orifice.

100-0.3 represents data for experiments at 100 psi through 0.3 mm orifice.

100-0.6 represents data for experiments at 100 psi through 0.6 mm orifice.

Volume in a Size Range = (% In a Size Range)* (Total Number of Particles)*$D^3/6$

Lower Size (microns)	Upper Size (microns)	Average Size (microns)	Total Volume in a Size Range			
			100-0.6	100-0.3	100-0.1	Base
0.1	0.12	0.11	25831.1	64304.9	335780	772.864
0.12	0.14	0.13	107919	286890	1399749	1491.61
0.14	0.16	0.15	282279	773685	3718240	2623.04
0.16	0.18	0.17	543509	1530909	7222466	5047.27
0.18	0.22	0.20	2174174	6321617	2.9E+07	23012.2
0.22	0.25	0.24	2832407	8352684	3.6E+07	35592.1
0.25	0.29	0.27	5227569	1.5E+07	6.3E+07	140140
0.29	0.34	0.32	7997072	2.2E+07	8.6E+07	654208
0.34	0.4	0.37	1E+07	2.6E+07	9.6E+07	2380368
0.4	0.46	0.43	9199756	2.2E+07	8.1E+07	5082620
0.46	0.54	0.50	1E+07	2.3E+07	8.7E+07	1.1E+07
0.54	0.63	0.59	8921311	1.8E+07	7.2E+07	1.5E+07
0.63	0.74	0.69	7080068	1.3E+07	6E+07	1.9E+07
0.74	0.86	0.80	3720608	6335219	4.6E+07	1.8E+07
0.86	1	0.93	1489379	2203267	3.8E+07	1.8E+07
1	1.2	1.10	558007	817169	2.7E+07	1.8E+07
1.2	1.4	1.30	153511	207515	7060525	9145930
1.4	1.6	1.50	58955.5	0	2033677	2894389
1.6	1.8	1.70	85821.8	0	0	1119177
1.8	2.2	2.00	1397464	0	0	2143992
2.2	2.5	2.35	2040313	0	0	3014317
2.5	2.9	2.70	2406800	0	0	4571688
2.9	3.4	3.15	545987	0	0	977263
TOTAL VOLUME			*7.7E+07*	*1.6E+08*	*7.4E+08*	*1.3E+08*

$\%\ In^*_i$ (Normalized % In a Size Range)= $\%\ In_i/V_T$

Lower Size (microns)	Upper Size (microns)	Average Size (microns)	% In* (Normalized % In a Size Range)			
			100-0.6	100-0.3	100-0.1	Base
0.1	0.12	0.11	0.44146	0.51774	0.59915	0.00779
0.12	0.14	0.13	1.11735	1.39936	1.51313	0.00911
0.14	0.16	0.15	1.90251	2.4566	2.61649	0.01043
0.16	0.18	0.17	2.51642	3.33923	3.49136	0.01378
0.18	0.22	0.2	6.18197	8.46802	8.5364	0.03859
0.22	0.25	0.235	4.96449	6.8971	6.61875	0.03679
0.25	0.29	0.27	6.0413	8.24838	7.55754	0.09552
0.29	0.34	0.315	5.81998	7.5282	6.55101	0.2808
0.34	0.4	0.37	4.50833	5.39702	4.50981	0.63046
0.4	0.46	0.43	2.63204	2.90601	2.41662	0.85763
0.46	0.54	0.5	1.88781	1.93279	1.6467	1.16665
0.54	0.63	0.585	1.01364	0.94691	0.85006	1.03147
0.63	0.74	0.685	0.50106	0.42917	0.44554	0.77973
0.74	0.86	0.8	0.1653	0.1326	0.21228	0.48011
0.86	1	0.93	0.04212	0.02935	0.11258	0.29375
1	1.2	1.1	0.00954	0.00658	0.04818	0.17965
1.2	1.4	1.3	0.00159	0.00101	0.00763	0.05585
1.4	1.6	1.5	0.0004	0	0.00143	0.01151
1.6	1.8	1.7	0.0004	0	0	0.00306
1.8	2.2	2	0.00397	0	0	0.0036
2.2	2.5	2.35	0.00358	0	0	0.00312
2.5	2.9	2.7	0.00278	0	0	0.00312
2.9	3.4	3.15	0.0004	0	0	0.00042

Figure 4 is the plot of % In* versus Average Diameter from the table above.

REFERENCES

1. Husemann I. H. K., I. R. wolf, I. R. Herrmann, R. N. B. Hoffmann, " Enhancing the Effectiveness of Dry Ultrafine Grinding and Classifying Processes by Addition of Surfactants", *Aufbereitungs-Technik*, 35, 1994, pp. 393-403.

2. Rawers J., R. Krabbl, N. Duttlinger, "Nanostructure Chracterization and Consolidated Iron Alloy", *Material Science Engineering*, A230, 1997, pp 139-145.

3. Endo Y., S. Hasebe, Y. Kousaka, " Dispersion of Aggregates of Fine Powder by Acceleration in an Air Stream and its Application to the Evaluation of Adhesion Between Particles" *Powder Technology*, 91, 1997, pp 25-30.

4. Higashitani, K., N. Tanise, A. Yoshiba, A. Kondo, H. Murata, "Dispersion of Coagulated Particles by Contractile Flow to Orifice", *Journal of Chemical Engineering of Japan*, 25, 1992, pp. 502-507.

5. Okubo, M. , M. Ito Fukami," Effect of Molecular Weight on Preparation of Nanoparticles by Particle Dissolution Method from Submicron-Sized Ionized Styrene – Methacrylic Acid Copolymer Particles in Nonionic Emulsifier Solution", *Journal of Applied Polymer Science*, 66, 1997, pp. 1461 – 1464.

6. Crawford, J.W., B.D. Sleeman, M. Young, "On the Relationsh Between Number-Size Distributions and the Fractal Dimension of Aggregate", *Journal of Soil Science*, 44, 1993, pp. 555 –565.

7. Meakin, P., " Diffusion-Controlled Cluster Formation in Two, Three and Four Dimensions." *Phys. Rev.*, 1983, A27:604.

8. Horwatt, S. W., D. L. Feke, I. Manas-Zlocozower, " The influence of Structural Heterogeneities on the Cohesivity and Breakup of Agglomerates in Simple Shear Flow", *Powder Technology*, 72, 1992, pp. 113-119.

9. Bang P. S., D. M. Smith, S. G. Thoma, "Determination of Agglomerate Strength Distributions, Part 4 Analysis of Multimodal Particle size Distributions", *Powder Technology*, 76, 1992, pp. 125-133.

10. Happel J., H. Brenner, *Low Reynolds Number Hydrodynamics*, Prentice Hall, Princeton, 1965.

11. Fuchs, N. A., *Progress in Aerosol Mechanics*, Izdatelstvo Akademii Nauk, USSR, Moscow, 1961. (in Russian).

12. Knudsen J. G., D. L. Katz, *Fluid Dynamics and Heat Transfer*, McGraw-Hill, New-York, 1958.